



Contents lists available at ScienceDirect

Chemical Engineering Research and Design

IChemE

journal homepage: [www.elsevier.com/locate/cherd](http://www.elsevier.com/locate/cherd)

## A detailed model for transport processes in a methane fed planar SOFC

E. Vakouftsi<sup>a</sup>, G. Marnellos<sup>a,b</sup>, C. Athanasiou<sup>a,b</sup>, F.A. Coutelieres<sup>a,c,\*</sup><sup>a</sup> Dept. of Engineering and Management of Energy Resources, University of Western Macedonia, Bakola & Sialvera, 50100 Kozani, Greece<sup>b</sup> Chemical Process Engineering Research Institute, Centre for Research & Technology, 6th km. Charilaou–Thermi Rd., 57001 Thermi, Thessaloniki, Greece<sup>c</sup> National Centre for Scientific Research “Demokritos”, 15310 Aghia Paraskevi Attikis, Greece

### ABSTRACT

In the present work the basic transport processes occurring in a planar solid oxide fuel cell (SOFC) were simulated. The Navier–Stokes and energy equations, including convective and diffusive terms, were numerically solved by the commercial CFD-ACE+ program along with the mass and charge transport equations. To achieve this, a three-dimensional geometry for the planar fuel cell has been built. It was also assumed that the feedstream was a mixture of methane and steam in a ratio avoiding carbon formation. In accordance with the literature, the steam reforming reaction, the water–gas shift reaction as well as electrochemical reactions were introduced to the model. The spatial variation of the mixture’s velocity, the temperature profiles and the species concentrations (mass fractions) were obtained. Furthermore, the effect of temperature on the produced current density was investigated and compared to the outcomes from isothermal imposed conditions.

© 2010 The Institution of Chemical Engineers. Published by Elsevier B.V. All rights reserved.

**Keywords:** Internal methane reforming; SOFC; Heat transfer; Modeling

### 1. Introduction

The increased energy demands worldwide and the intense environmental impact have imposed the necessity of substituting conventional energy systems based on fossil fuels and combustion processes with power plants based on renewable energy sources (RES). Fuel cells seem to be an attractive solution since they can convert fuel’s chemical energy into electricity with high performances and low emissions (almost zero pollutants) because such devices are not restricted by the Carnot limitations. The majority of the fuel cell systems nowadays operate with hydrogen which is neither cheap nor easy to store. However, the high operational temperature (873–1473 K) and the materials used in solid oxide fuel cells (SOFCs) allow fuel flexibility in feedstream such as carbon monoxide, natural gas and hydrocarbons (Douvartzides et al., 2004; Jeng

and Chen, 2002; Coutelieres et al., 2003; Hernandez-Pacheco et al., 2005; Aloui and Halouani, 2007). The advantage of such a choice is that these fuels can be naturally found and easily stored and transported in opposition to hydrogen which is a highly demanding energy carrier. In the current simulation, a mixture of methane and steam was introduced to the fuel cell in a ratio preventing carbon formation, while internal methane reforming and water–gas shift reaction have been implemented as well (Park et al., 1999; Demin et al., 1992; Lehnert et al., 2000; Hou and Hughes, 2001; Xu and Froment, 1989; Morel et al., 2005; Ahmed and Fogger, 2000; Achenbach and Riensche, 1994; Nikooyeh et al., 2007; Ho et al., 2009). A three-dimensional model was created and the fundamental transport processes have been examined. Furthermore, the effect of temperature on the produced current density for isothermal and non-isothermal conditions was investigated.

\* Corresponding author at: Department of Environmental and Natural Resources Management, University of Ioannina, Seferi 2, 30100 Agrinio, Greece. Tel.: +30 2641074196; fax: +30 2641074176.

E-mail addresses: [evakouftsi@uowm.gr](mailto:evakouftsi@uowm.gr) (E. Vakouftsi), [gmarnellos@uowm.gr](mailto:gmarnellos@uowm.gr) (G. Marnellos), [costath@cperi.certh.gr](mailto:costath@cperi.certh.gr) (C. Athanasiou), [fcoutelieres@uowm.gr](mailto:fcoutelieres@uowm.gr) (F.A. Coutelieres).

Received 22 April 2009; Received in revised form 27 April 2010; Accepted 19 May 2010

0263-8762/\$ – see front matter © 2010 The Institution of Chemical Engineers. Published by Elsevier B.V. All rights reserved.

doi:10.1016/j.cherd.2010.05.003

## 2. Theory

The fundamental transport phenomena occurring in a fuel cell are the flow, the heat transfer, the mass transport and the charge exchange. Since laminar conditions are usually assumed, the flow can be well described by the Navier–Stokes equations, which for incompressible fluids are given as:

$$\frac{\partial(\underline{u})}{\partial t} + (\underline{u} \cdot \nabla)\underline{u} = -\frac{1}{\rho}\nabla p + \nu(\nabla^2 \cdot \underline{u}) \quad (1)$$

where  $\underline{u}$  is the velocity vector,  $\rho$  is the density,  $p$  is the pressure and  $\nu$  is the kinematic viscosity. By neglecting radiation, the energy balance in the system can be written as:

$$\frac{\partial(\rho c_p T)}{\partial t} + (\underline{u} \cdot \nabla)(\rho c_p T) = [\nabla \cdot a \nabla(\rho c_p T)] - (\rho c_p T)(\nabla \cdot \underline{u}) + \dot{Q} \quad (2)$$

where  $T$  is the temperature,  $c_p$  is the heat capacity of the mixture,  $a$  is the thermal diffusivity coefficient and  $\dot{Q}$  is the amount of heat produced/consumed due to reactions. The species mass fractions at each point within the area of interest were obtained by numerically solving the convective diffusion equation where both surface and volume reactions take place:

$$\frac{\partial(\rho x_i)}{\partial t} + \nabla \cdot (\rho \underline{u} x_i) - \nabla \cdot (\rho D_{i,\text{mix}} \nabla x_i) + \dot{\omega} = 0 \quad (3)$$

where  $x_i$  is the species  $i$  mass fraction,  $D_{i,\text{mix}}$  is its thermal diffusivity coefficient and  $\dot{\omega}$  is the non linear terms representing the volumetric production/destruction rate of species  $i$  due to the reactions.

For the calculation of current density, the Butler–Volmer equation was used, written as follows:

$$I = I_0 \left[ \exp\left(\frac{a_a \eta F}{RT}\right) - \exp\left(-\frac{a_c \eta F}{RT}\right) \right] \quad (4)$$

where  $I_0$  is the exchange current density,  $a_a$ ,  $a_c$  are the anodic and cathodic charge transfer coefficients,  $F$  is the Faraday constant,  $\eta$  is the overpotential and  $R$  is the universal gas constant.

## 3. Simulation

It was assumed that  $\text{H}_2$  and  $\text{CO}$  were electrochemically oxidized at the three-phase boundary of the porous anode electrode according to the following reactions:



while the  $\text{O}^{2-}$  migrated from the surface reaction (oxygen reduction):



at the porous cathode electrode. In the present study we presumed that current inside the porous media can be split into two currents, one flowing through the fluid phase (pores) of the porous medium and the other flowing through the solid phase (matrix) (Newman and Tiedemann, 1975). For the electrochemical reactions, the values of the exchange current density used for the anode electrode,  $I_{0(a)}$ , and for the cathode electrode,  $I_{0(c)}$ , depended on temperature and are given in Table 1, where  $(S/V)$  is the ratio of the surface of the three-phase

**Table 1 – Reference current density.**

Temperature [K]	1073	1173	1273
$I_{0(a)}(S/V)$ [ $\text{Am}^{-3}$ ]	$2.28 \times 10^9$	$6.51 \times 10^9$	$1.58 \times 10^{10}$
$I_{0(c)}(S/V)$ [ $\text{Am}^{-3}$ ]	$1.31 \times 10^8$	$6.05 \times 10^8$	$2.74 \times 10^9$

boundary region to the volume (Achenbach, 1994). Moreover, the values of the charge transfer coefficients were  $\alpha_a = \alpha_c = 0.7$  (Ramakrishna et al., 2006).

The hydrogen and the carbon monoxide were produced by the methane steam reforming reaction:



which was assumed to take place only at the porous anode. The relative kinetics [ $\text{kmol m}^{-3} \text{s}^{-1}$ ] in Arrhenius form can be written as (Klein et al., 2007a):

$$r_{\text{STR}} = \left( 1.91 \times 10^8 T^2 \exp\left(-\frac{27,063}{T}\right) [\text{CH}_4][\text{H}_2\text{O}] \right) - \left( 1.1 \times 10^{-7} T^4 \exp\left(-\frac{232.78}{T}\right) [\text{H}_2]^3 [\text{CO}] \right) \quad (8)$$

where  $[i]$  are the species  $i$  concentrations.

It was also assumed that the water–gas shift reaction (WGS), given as:



occurred at the porous electrodes and at the gas phase, i.e. wherever the relative gases were present, while the relative kinetics [ $\text{kmol m}^{-3} \text{s}^{-1}$ ] can be described in Arrhenius form as (Klein et al., 2007a):

$$r_{\text{WGS}} = \left( 1,199 T^2 \exp\left(-\frac{12,500}{T}\right) [\text{H}_2\text{O}][\text{CO}] \right) - \left( 1,119 T^2 \exp\left(-\frac{12,500}{T}\right) [\text{H}_2][\text{CO}_2] \right) \quad (10)$$

Regarding the boundary conditions, the mass flow rates for the anodic and the cathodic mixtures were assumed to be constant and equal to  $2.0 \times 10^{-6} \text{ kg/s}$  and  $2.12 \times 10^{-6}$  for the anode and cathode channels, respectively, while pressure of 1 atm was set at the inlets and outlets. Considering no accumulation, zero mass flux was set at the walls and at the outlets. Additionally, preheated fuel and air mixtures (1073, 1173, and 1273 K) entered the fuel cell, while zero heat flux was set at all the other boundaries. Finally, constant value of zero potential was set to the anode collector, while the potential of the cathode collector varied from 0.1 to 0.7 V.

For the current simulation, a planar SOFC was considered which consisted of seven separated volumes: the fuel and air channel where the corresponding mixtures were introduced, the porous anode and cathode electrodes where the reactions occurred, the dense electrolyte through which oxygen ions ( $\text{O}^{2-}$ ) migrate to reach anode electrode and finally the anode and cathode collectors. A two dimensional cut of the fuel cell is depicted in Fig. 1, where the dimensions have been chosen in accordance with Ramakrishna et al. (2006). The feeding stream was assumed to be a mixture of 37% methane and 63% steam on %wt basis, while typical composition for the atmospheric air (22%  $\text{O}_2$  and 77%  $\text{N}_2$  on %wt basis, as well) was applied at the cathode channels. Both electrodes were modeled as isotropic

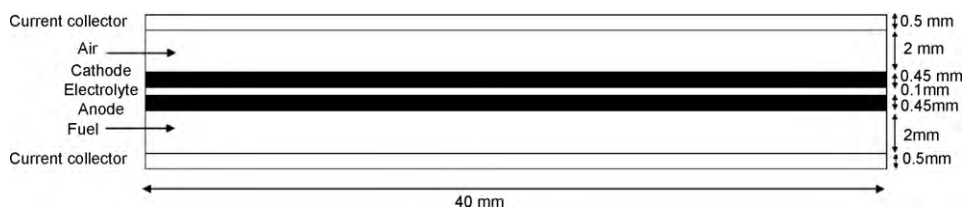


Fig. 1 – Simulated SOFC geometry.

Table 2 – Porous media properties.

	Anode	Electrolyte	Cathode
$\varepsilon$ (porosity)	0.40	0.01	0.50
$\kappa$ (permeability)	$1e^{-12}$	$1e^{-18}$	$1e^{-12}$
$d_p$ (mean pore diameter) [m]	$1e^{-6}$	$1e^{-6}$	$1e^{-6}$
$k$ (thermal conductivity) [ $Wm^{-1}K^{-1}$ ]	6.23	2.7	9.6
$S/V$ (surface to volume ratio) [ $m^{-1}$ ]	$3e^6$	–	$3e^6$
$\sigma_F$ (electronic phase conductivity) [ $\Omega^{-1}m^{-1}$ ]	100,000	$1e^{-20}$	7,700
$\sigma_S$ (ionic phase conductivity) [ $\Omega^{-1}m^{-1}$ ]	10	10	10

porous media and their physical characteristics are listed in Table 2 (Ramakrishna et al., 2006; Klein et al., 2007a).

Furthermore, it was assumed that the gases followed the ideal law of gases for the calculation of density [ $kg\ m^{-3}$ ] and the kinetic theory of gases was used to estimate the viscosity [ $kg\ m^{-1}\ s^{-1}$ ]. The specific heat  $c_p$  [ $J\ kg^{-1}\ K^{-1}$ ] derived by fittings to the experimental JANNAF curves and the mass diffusivity [ $kg\ m^{-1}\ s^{-1}$ ] was calculated by a Schmidt number equal to 0.7. The numerical solution for the above mentioned equations was obtained by the commercial package CFD-ACE<sup>+</sup>, which is based on the finite volume method, applying all the appropriate boundary conditions in order to achieve residual values for all the quantities less than  $10^{-4}$ . The three-dimensional fuel cell was discretized in space by structured grid consisting of 33,516 cells.

## 4. Results and discussion

Since the majority of the available simulations in the relative literature deals with isothermal conditions (Bhattacharyya et al., 2007; Wang et al., 2008), the current work apart from examining this standard case, aims at the investigation of the effect of temperature variation along the fuel cell on different model parameters such as velocity, species mass fractions and produced current density.

All the typical distributions for the main physical quantities (velocity, temperature and mass fractions) were obtained for constant gas inlet temperature (1273 K) for both fuel and air mixtures and are presented below in contour plot in a two dimensional cut in the middle plane of the fuel cell.

### 4.1. Isothermal conditions

Fig. 2 shows the developed velocity profile, which is obviously parabolic for both flow channels, satisfying the non-slip boundary condition applied on the wall.

The consumption of  $CH_4$  and steam due to the methane steam reforming reaction along the fuel cell length is depicted in Fig. 3a and b, respectively, where the reduction of their mass fractions is observed. It is worth mentioning that the reaction kinetics is rather small, since at the cell outlet the  $CH_4$  as well as the steam mass fractions are still high. As far as hydrogen and carbon monoxide are concerned, it is rather clear that they

are produced at the anode and their production rate is higher than their consumption. (Fig. 4a and b).

At the same time, a small depletion of  $O_2$  can be seen in the cathode electrode and in the cathode channel which is attributed to the electrochemical reactions. The  $O_2$  gradient is quite small since its mass flow rate is high enough to avoid oxygen depletion that would reduce fuel cell's performance, while the highly convective regime could be considered as an extra barrier to the extent of the electrochemical reactions (Fig. 5).

### 4.2. Non-isothermal conditions

The velocity profiles for both channels were also parabolic and the maximum values obtained were very close to the ones recorded for the isothermal case (Fig. 6). For the methane and steam mass fraction profiles it is worth mentioning that their consumption is quite smaller compared to the previous case due to the reduced methane steam reforming kinetics which is a function of temperature (Fig. 7a and b). When isothermal conditions are assumed, a specific amount of energy is imposed, which is mainly consumed to keep active the strongly endothermic reforming reaction. As a result, smaller  $H_2$  and  $CO$  mass fractions were achieved (Fig. 8a and b). Oxygen mass fraction follows the same trend and slightly smaller consumption is evident (Fig. 9).

All the above results can be clarified by the temperature profile depicted in Fig. 10, where the temperature along the fuel cell decreases implying lower kinetics for the reactions involved. This result is in accordance with other scientific studies (Klein et al., 2007b) although some other researchers reported increment of temperature throughout the fuel cell length (Nikooyeh et al., 2007; Ho et al., 2009). This discrepancy can be attributed to the relative strengths of the convective regime used in the present work: although the electrochemical reactions are exothermic, the strongly endothermic methane steam reforming reaction accompanied by the relatively high-flow rate, entail the cooling of the system.

### 4.3. Effect of temperature

Three different values for the inlet temperature were examined allowing in the first case spatial temperature variation

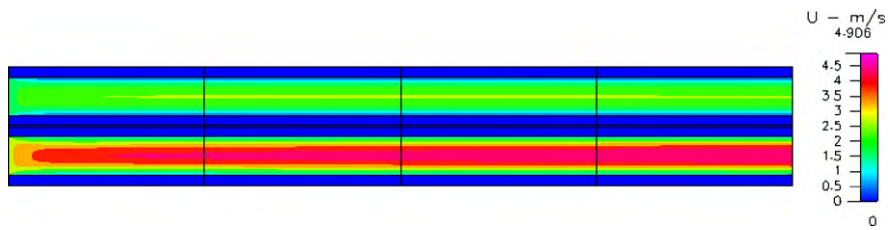


Fig. 2 – Velocity profile for isothermal conditions.

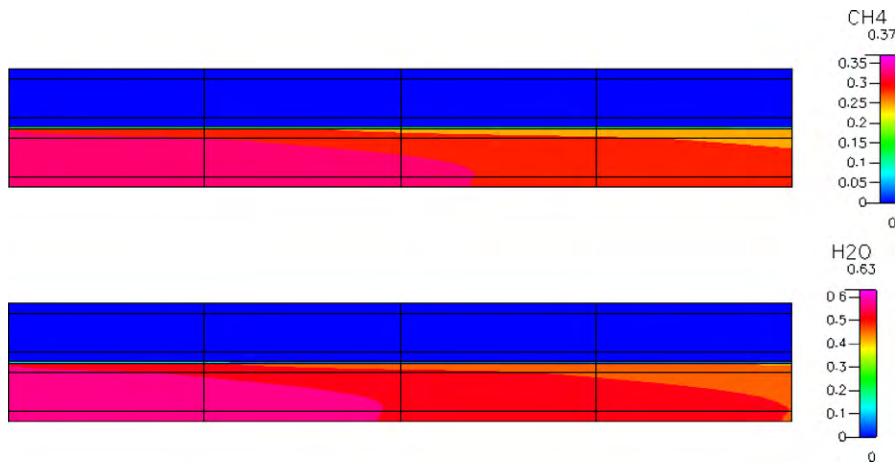


Fig. 3 – Mass fraction profiles for (a) methane and (b) steam (isothermal conditions).

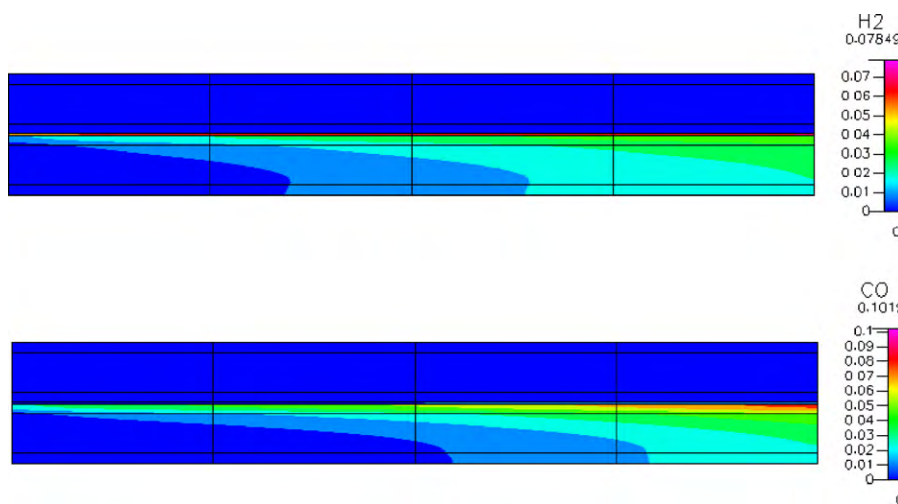


Fig. 4 – Mass fraction profile for (a) hydrogen and (b) carbon monoxide (isothermal conditions).

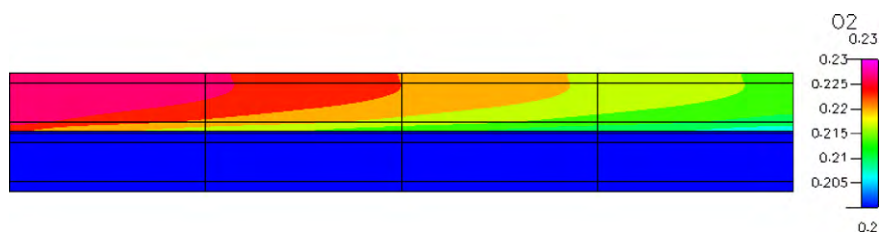


Fig. 5 – Mass fraction profile for oxygen (isothermal conditions).



Fig. 6 – Velocity profile for non-isothermal conditions.

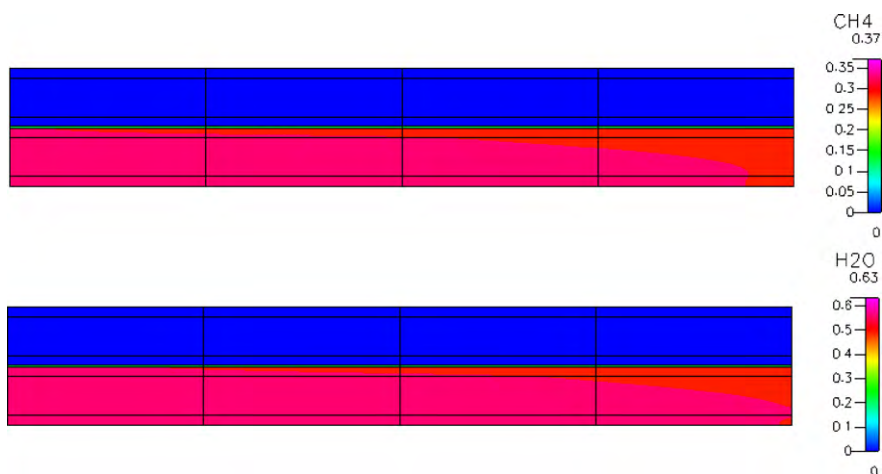


Fig. 7 – Mass fraction profile for (a) methane and (b) steam (non-isothermal conditions).

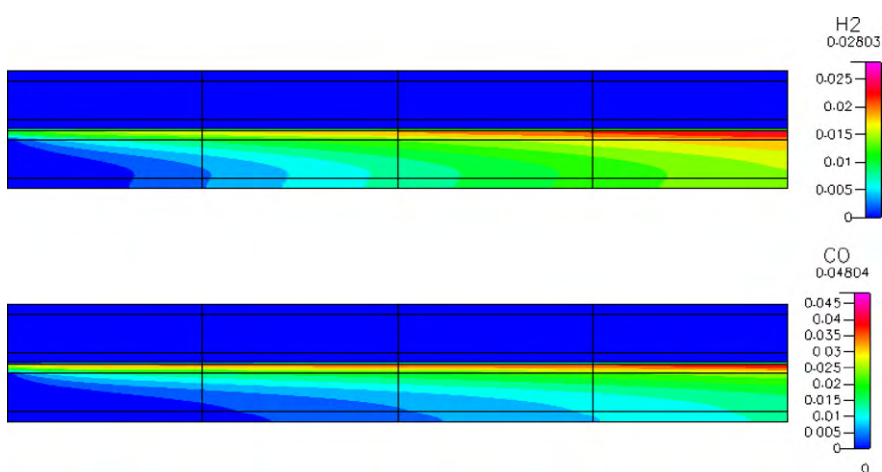


Fig. 8 – Mass fraction profile for (a) hydrogen and (b) carbon monoxide (non-isothermal conditions).

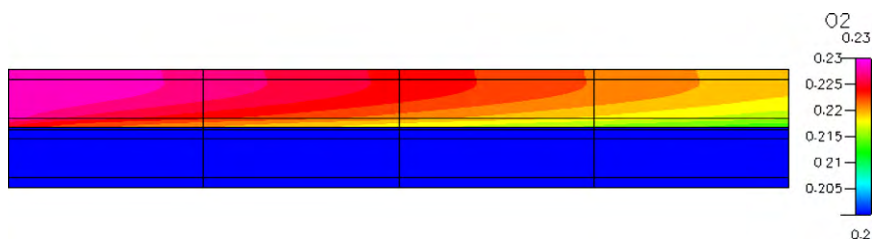


Fig. 9 – Mass fraction profile for oxygen (non-isothermal conditions).

along the fuel cell (due to reactions) and in the second case imposing isothermal conditions throughout the fuel cell. The results referring to the current density are presented in Fig. 11. It can be observed that the increase in overpotential for every case results in higher current densities, since the kinetics of oxygen ions are reinforced and more H<sub>2</sub> and CO species react. Moreover, the increase of the mixture's inlet tempera-

ture contributes to faster kinetics for all the reactions and as a result more current is produced mainly because of the higher energetic content of the feeding stream. It should be outlined that maintaining the temperature constant along the fuel cell yields in higher current density values since the reduction of temperature due to methane steam reforming reaction was not high enough to influence the overall cell output.

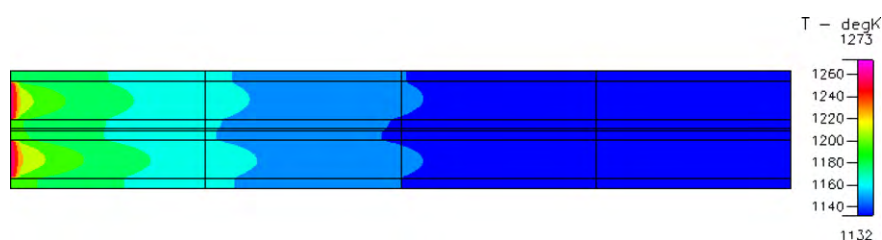


Fig. 10 – Temperature profile for non-isothermal conditions.

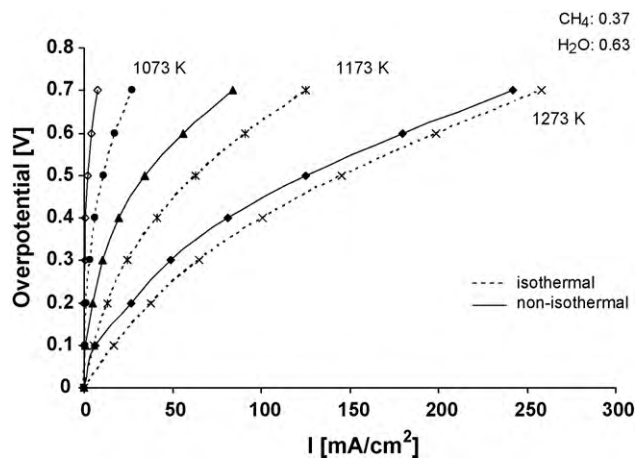


Fig. 11 – Temperature effect on current density for isothermal and non-isothermal conditions.

## 5. Conclusions

In the current study the performance of a methane/steam fed planar SOFC was examined and the fundamental transport processes were simulated for isothermal and non-isothermal conditions. It was found that the velocity profiles for the both cases were parabolic satisfying the non-slip boundary condition, while the methane and the steam were consumed at the anode electrode due to the methane steam reforming reaction and at the same time, hydrogen and carbon monoxide were produced at the anode electrode. Their profiles are a combined contribution of all the reactions taken into account, i.e. electrochemical, surface methane reforming and water–gas shift. The increased kinetics due to higher temperature values at the fuel cell reinforce the oxygen ions kinetics and therefore increase the current density production for any temperature of the inlet mixtures. Finally, it could be concluded that higher and constant thermal conditions correspond to consequently

improved performance for the SOFC compared to the non-isothermal conditions.

## References

- Achenbach, E., 1994, *J. Power Sources*, 49: 333.  
 Achenbach, E. and Riensche, E., 1994, *J. Power Sources*, 52: 283.  
 Ahmed, K. and Foger, K., 2000, *Catal. Today*, 63: 479.  
 Aloui, T. and Halouani, K., 2007, *Appl. Therm. Eng.*, 27: 731.  
 Bhattacharyya, D., Rengaswamy, R. and Finnerty, C., 2007, *Chem. Eng. Sci.*, 62: 4250.  
 Coutelieris, F.A., Douvartzides, S. and Tsiakaras, P., 2003, *J. Power Sources*, 123: 200.  
 Demin, A.K., Alderucci, V., Ielo, I., Fadeev, G.I., Maggio, G., Giordano, N. and Antonucci, V., 1992, *Int. J. Hydrogen Energy*, 17: 451.  
 Douvartzides, S.L., Coutelieris, F.A., Demin, A.K. and Tsiakaras, P.E., 2004, *Int. J. Hydrogen Energy*, 29: 375.  
 Hernandez-Pacheco, E., Singh, D., Hutton, P.N., Patel, N. and Mann, M.D., 2005, *Int. J. Hydrogen Energy*, 30: 1221.  
 Ho, T.X., Kosinski, P., Hoffmann, A.C. and Vik, A., 2009, *Chem. Eng. Sci.*, 64: 3000.  
 Hou, K. and Hughes, R., 2001, *Chem. Eng. J.*, 82: 311.  
 Jeng, K.T. and Chen, C.W., 2002, *J. Power Sources*, 112: 367.  
 Klein, J.-M., Bultel, Y., Pons, M. and Ozil, P., 2007, *J. Fuel Cell Technol.*, 4: 425.  
 Klein, J.-M., Bultel, Y., Georges, S. and Pons, M., 2007, *Chem. Eng. Sci.*, 62: 1636.  
 Lehnert, W., Meusinger, J. and Thom, F., 2000, *J. Power Sources*, 87: 57.  
 Morel, B., Laurencin, J., Bultel, Y. and Lefebvre-Joud, F., 2005, *J. Electrochem. Soc.*, 152: A1382.  
 Newman, J. and Tiedemann, W., 1975, *AIChE J.*, 21: 25.  
 Nikooyeh, K., Jeje, A.A. and Hill, J.M., 2007, *J. Power Sources*, 171: 601.  
 Park, S., Carcium, R., Vohts, J.M. and Gorte, R.J., 1999, *J. Electrochem. Soc.*, 10: 3603.  
 Ramakrishna, P.A., Yang, S. and Sohn, C.H., 2006, *J. Power Sources*, 158: 378.  
 Wang, L., Zhang, H. and Weng, S., 2008, *J. Power Sources*, 177: 579.  
 Xu, J. and Froment, G.F., 1989, *AIChE J.*, 35: 88.